Journal of Cleaner Production 241 (2019) 118412

Contents lists available at ScienceDirect

Journal of Cleaner Production

journal homepage: www.elsevier.com/locate/jclepro

Evaluation of the energy recovery potential of thermoelectric generators in diesel engines

Rafael Ramírez [a, b], Alexis Sagastume Gutiérrez [a], Juan J. Cabello Eras [a], Karen Valencia [b], Brando Hernández [b], Jorge Duarte Forero [b, *]

[a] Universidad de la Costa CUC, Calle 58 Número 55 - 66, Barranquilla, Colombia
[b] Universidad del Atlántico, Grupo Kaí, Departamento de Ingeniería Mecánica, Carrera 30 Número 8 - 49, Puerto Colombia, Área Metropolitana de Barranquilla, Colombia

ARTICLE INFO

Article history:
Received 2 February 2019
Received in revised form
7 September 2019
Accepted 11 September 2019
Available online 12 September 2019

Handling Editor: Cecilia Maria Villas Bôas de Almeida

Keywords:
Energy recovery
Heat exchanger
Thermoelectric generator
Thermoelectric module
Internal combustion engine

ABSTRACT

Thermoelectric generation is an alternative to recover some of the wasted energy trough an exhaust of the internal combustion engines. This paper assesses the performance of a thermoelectric generator with 20 modules by implementing a waffle heat exchanger. Experimental results showed a variable range of power recovery from 57.87 W to 71.13 W for B10, B5, and Diesel. The highest energy conversion efficiency of the aforementioned thermoelectric device was of 3% with the highest load and the fastest rotational speed. Also, the recovery process reduced gaseous emissions such as CO, CO_2, NO, NO_X, and HC. Additionally, the smoke opacity per kWh is reduced at significant levels of operations such as 2.42% when using diesel, 2.65% when using B5 and 3% when using B10. However, when using biodiesel blends, NOx emissions were increased. Overall the biodiesel resulted in a higher power recovery performance versus the diesel.

1. Introduction

The growing energy demand, currently supported by limited reserves of fossil fuels, drives the most significant energy security and environmental issues worldwide (Verma et al., 2017). Internal combustion engines (ICEs) are the main consumers of fossil fuel as a primary energy source, and they are widespread in the transport sector, industrial and agricultural machinery, and stationary power units (Alagumalai, 2014; Rimkus et al., 2017). Combustion products from ICEs include CO_2, CO, CH_4, and NO_X, which stand as the main greenhouse gases (GHG) affecting climate change and global warming among other environmental impacts (Rimkus et al., 2017). The increasing of the environmental concerns and a decreasing in fossil fuel reserves represent significant challenges to the automotive industry in searching for higher energy efficiency and lower environmental pollution (Darda et al., 2019; Verma et al., 2017). The growing energy demand, currently supported by limited reserves of fossil fuels, drive the most significant energy security and environmental issues worldwide (Verma et al., 2017). Internal combustion engines (ICEs), the main consumers of fossil fuel as a primary energy source, are widespread in the transport sector, industrial and agricultural machinery, and stationary power units (Alagumalai, 2014; Rimkus et al., 2017). Combustion products from ICEs include CO_2, CO, CH_4, and NO_X, which stand as the main greenhouse gases (GHG) affecting climate change and global warming among other environmental impacts (Rimkus et al., 2017). The increasing environmental concerns and the decreasing reserves of fossil fuels, stand as significant challenges to the automotive industry, driving the search for higher energy efficiency and lower environmental pollution (Darda et al., 2019; Verma et al., 2017).

Different approaches have been developed in ICEs to get higher energy efficiency with lower environmental impacts:

- Continuous variable valve timing system (CVVT): This system improves the energy efficiency at partial loads up to 4.1%, although it introduces charge dilution effects that reduce the

* Corresponding author.
E-mail address: jorgeduarte@mail.uniatlantico.edu.co (J. Duarte Forero).

https://doi.org/10.1016/j.jclepro.2019.118412
0959-6526/

Nomenclature

W	Power [W]
V	Voltage [V]
I	Electric current [A]
L	Length [m]
$\mathbf{L_{equiv}}$	Equivalent length [m]
$\dot{\mathbf{m}}$	Mass flow rate [kg /s]
$\mathbf{P_{pum}}$	Pumping power [W]
NCP	Net caloric power [MJ /kg]
T	Temperature [K]
α	Seebeck coefficient [μV /K]
K	Thermal conductance [W /K]
R	Electrical resistance [Ω]
K	Thermal conductivity [W /cm ·K]
n	Number of thermocouples
ρ	Electrical resistivity [Ω ·cm]
q	Heat [W]
A	Area [mm^2]
c	Specific heat [J /kg ·K]
η	Efficiency

maximum power in about 35.7% (Osorio and Rivera-Alvarez, 2018).

- Injecting air bubbles into the engine cooling system: although it improves the energy efficiency up to 5.69%, under some air injection conditions, it increases the fuel consumption (Zavaragh et al., 2017).
- Technologies to recover the heat wasted with the exhausts to preheat combustion air, fuel, and to feed an Organic Rankine Cycle or a thermoelectric generator (TEG) (Lion et al., 2017).

Regardless of these results, there are further potentials to improve the energy efficiency of ICEs. In particular, the use of thermoelectric generators has been recently discussed as an alternative towards higher efficiency standards (Aranguren et al., 2017; He and Wang, 2017). Thermoelectric generators either combine a heat exchanger with several thermoelectric modules (TEM) or they expose the TEMs directly to the exhaust (Niu et al., 2014; Vale et al., 2017). Thermoelectric generators transform heat into electricity, and their main advantage is their compactness and the absence of moving parts. The energy conversion efficiency (i.e., the heat transformed into electricity) of the thermoelectric devices is around 2% when the TEMs are directly exposed to the exhaust while introducing heat exchangers improve the conversion efficiency up to 2.8% (Kim et al., 2016, 2017).

Consequently, towards higher energy conversion efficiencies, the use of heat exchangers in TEGs has been considered (Kim et al., 2017; Temizer and Ilkiliç, 2016), and different designs have been discussed (Patil et al., 2018; Su et al., 2014). However, heat exchangers introduce pressure drops affecting the efficiency of the ICEs (In et al., 2015). Thus, a balance between the temperature gradient and the pressure drop is required to ensure higher fuel economies from the implementation of TEGs (Lan et al., 2018).

Moreover, the exhaust parameters vary during the operation of ICEs, which affects the performance of TEGs, so it is necessary to define properly the size and the exhaust flow direction of a TEG, to optimize the energy recovery during the operation of ICEs (He et al., 2015). Even though some studies have demonstrated the feasibility of using TEGs to recover heat from exhaust gases (Li et al., 2016), and different types of heat exchangers have been developed (Kiziroglou et al., 2014; Patil et al., 2018).

Although there are several specialized references in the literature focused on TEGs performance evaluation (Patil et al., 2018), to the best knowledge of the authors there are no studies addressing the influence of fuel mixes on the efficiency and performance of TEGs, and the reduction of greenhouse gas emissions in the ICE.

This paper aims in assessing the energy conversion performance of a TEG with waffle heat exchanger installed in a diesel ICE using fuel mixes with biodiesel. The experimental research also considering the variation of the exhaust parameters, the size of the TEG, the type, and size of heat exchanger (i.e., heat transfer area, temperature gradient, pressure drop, etc.), to improve the energy efficiency of an ICE. Additionally, this study aims to evaluate the economic and environmental implications of implementing a TEG in an ICE.

2. Materials and methods

2.1. Thermoelectric module (TEM)

A TEM is a device that transforms heat into electricity. The energy conversion rate of TEMs depends on the temperature gradient between its upper and lower surfaces (Love et al., 2012) (see Fig. 1). Thermoelectric modules are electrically connected in a serial arrangement.

Each TEM includes several thermocouples arranged between two ceramic plates of high thermal conductivity and low electrical conductivity (See Fig. 1a). Each of these thermocouples consists of one *p*-type and one *n*-type semiconductor electrically connected in a serial arrangement (Niu et al., 2014). This arrangement includes a hot surface to extract the heat (q_h) from the exhausts and a cold surface to reject the heat (q_c) towards ambient. Semiconductors are located between ceramic plates of high thermal conductivity and low electrical conductivity (Lee, 2010).

Considering the loss due to the electrical resistance and the heat conduction on the semiconductors, and using numerical methods, the heat transfer in the node "*i*" of the hot surface can be calculated as:

$$q_h^i = n_y \cdot \left[\alpha_{pn} \cdot T_h^i \cdot I - 0.5 \cdot R_{pn} \cdot I^2 + K_{pn} \cdot \left(T_h^i - T_c^i\right)\right] \quad (1)$$

While the heat transfer in the node "k" of the cold surface is calculated as:

$$q_c^k = n_y \cdot \left[\alpha_{pn} \cdot T_c^k \cdot I + 0.5 \cdot R_{pn} \cdot I^2 + K_{pn} \cdot \left(T_h^k - T_c^k\right)\right] \quad (2)$$

Where α_{pn} is the Seebeck coefficient, K_{pn} is the thermal conductance, $R_{pn}$is the electrical resistance of a thermocouple, and n_y is the number of thermocouples in the TEM.

The values of α_{pn} , K_{pn} , R_{pn}, are calculated as:

$$\alpha_{pn} = \alpha_p - \alpha_n \quad (3)$$

$$K_{pn} = \frac{A \cdot (k_p + k_n)}{L} \quad (4)$$

$$R_{pn} = \frac{L \cdot (\rho_p + \rho_n)}{A} \quad (5)$$

The heat absorbed by the hotter surface of the TEM balances the heat transferred by the exhausts, which is the hot flow (f), while the heat rejected in the cold surface of the TEG balances the heat transferred to the ambient, absorbed by the cold flow (c). The cold fluid is the atmospheric air that is in contact with the cold surface. Therefore, the following equations can be used:

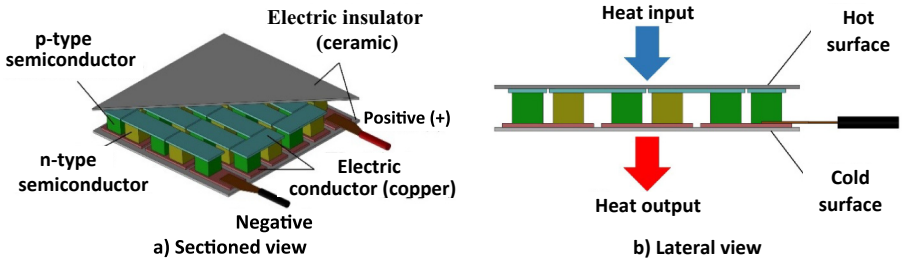

Fig. 1. Thermoelectric module.

$$q_h^i = c_f \cdot \dot{m}_f \cdot \left(T_f^i - T_f^{i+1}\right) \tag{6}$$

$$q_c^k = c_c \cdot \dot{m}_c \cdot \left(T_c^{k+1} - T_c^k\right) \tag{7}$$

where c_f and c_c are the specific heats of the hot and cold fluids, respectively.

From the energy balance of the TEM, the output power of a TEM can be calculated as:

$$W_{TEM} = \sum_{i=1}^{n_x} \left(q_h^i - q_c^i\right) \tag{8}$$

In this analysis, a TEM mode l TEG1-12610-5.1 that can operate up to 300 °C on the hot side, is used.

2.2. Heat exchanger

Although heat exchangers improve the energy conversion efficiency of TEGs, they introduce pressure drops. Thus, it is essential a balance between the pressure drop and the higher heat transfer rate resulting from the introduction of heat exchangers. Therefore, the adequate selection of heat exchangers is the cornerstone to maximize the heat transfer from the exhaust while keeping the pressure drop within the adequate values. Fig. 2 shows the main designs of heat exchangers used for TEGs.

The rectangular heat exchanger of Fig. 2a has a low heat transfer coefficient, which is the result of a low resident time of the exhaust (Kim et al., 2016). Moreover, the offset strip heat exchanger of Fig. 2b significantly increases the heat transfer rate as compared to the rectangular heat exchanger that generates a significant pressure drop (Vale et al., 2017). Finally, the waffle heat exchanger, as shown in Fig. 2c increases the heat transfer coefficient concerning the rectangular heat exchanger while generating a lower pressure drop than the offset strip fins heat exchanger.

OpenFOAM® fluid dynamics software was used to generate a CFD simulation to compare pressure drops in different heat exchanger designs. In this simulation a mesh with hexahedral elements for flat surfaces, while tetrahedral elements were used in the analysis of curvature regions. The exhaust flow in the heat exchanger was considered fully turbulent, and it was modeled using the k - ε model.

Table 1 shows the operating characteristics of the engine used for this analysis. Thus, 300 °C at 20 m/s is used in the simulation as the exhaust inlet temperature to the heat.

The results of the simulations show that the offset strip heat exchanger causes a pressure drop over 2 kPa, which surpasses the maximum admissible pressure drop of the test engine considered in this study. Moreover, the waffle heat exchanger induces a significantly lower pressure drop, while causing a higher heat transfer rate than the rectangular heat exchanger. Therefore, the waffle heat exchanger shows the best balance between pressure drop and heat exchange to improve the performance of TEGs. Additionally, the waffle heat exchanger has a simpler design than the offset strip fins heat exchanger, so it requires lower manufacturing costs. Therefore, this paper considers the waffle heat exchanger, as shown in Fig. 3 for this analysis. To further increase the heat transfer rate, the heat exchanger is manufactured with copper.

2.3. Thermoelectric generator (TEG)

Fig. 4 shows the thermoelectric generator device, which includes a heat exchanger, the TEMs, and a cooling system.

Twenty TEMs were assembled on the external surfaces of the

Table 1
Specifications of the diesel engine.

Engine type	1 cylinder
Manufacturer	SOKAN
Model	SK-MDF300
Cycle	4 Strokes
Bore x stroke	78 mm × 62.57 mm
Displaced volume	299 CC
Compression ratio	20:1
Maximum power	4.6 hp at 3600 rpm
Intake system	Naturally Aspirated
Injection system	Direct injection
Injection Angle	20° BTDC

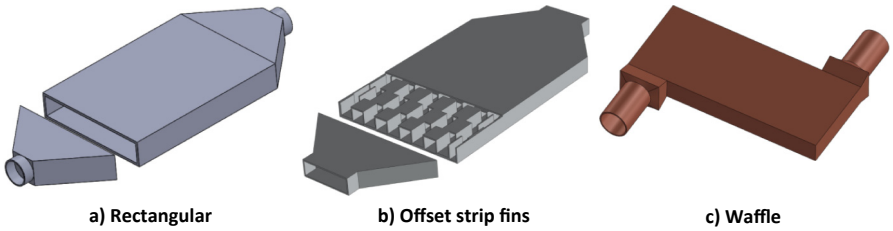

Fig. 2. Heat exchanger designs.

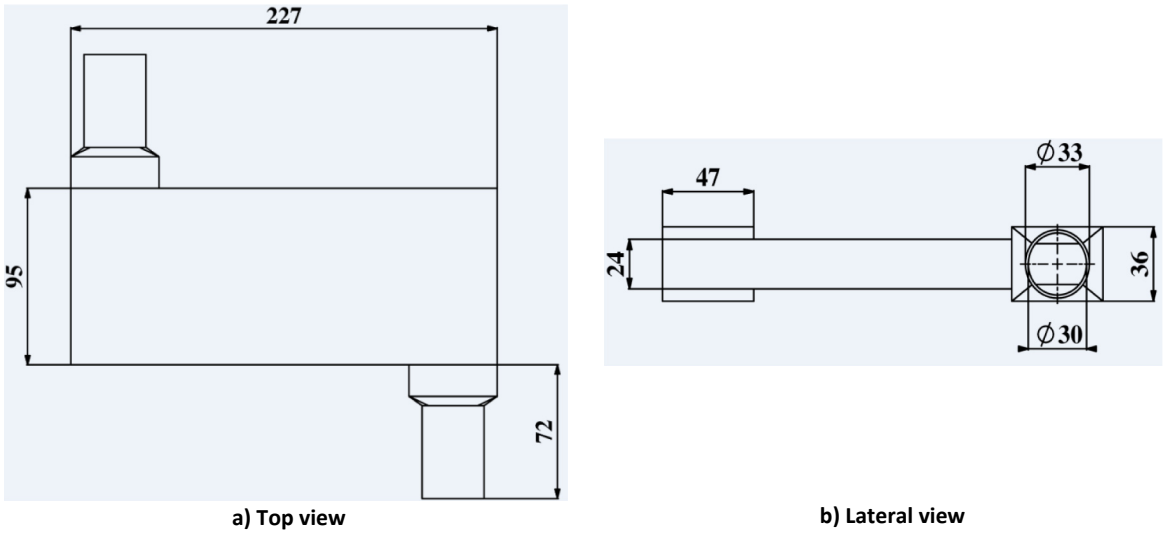

Fig. 3. Waffle heat exchanger dimensions (mm).

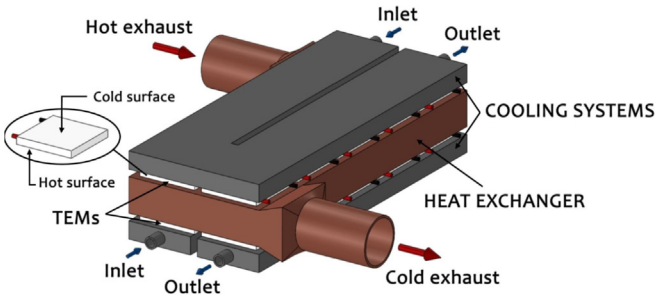

Fig. 4. Thermoelectric generator.

heat exchanger, as shown in Fig. 5. A thin layer of thermal paste between the external surface of the heat exchanger and the thermoelectric modules was used to enhance the heat conduction, and to compensate the mechanical tolerances in the device.

Thermoelectric modules 1 to 10, located in the upper surface, are symmetrical with TEMs 11 to 12 (i.e., they are exposed to the same temperatures thus yielding the same electricity) and only one surface of the heat exchanger will be analyzed. Furthermore, the waffles indicate the path of the exhaust in the heat exchanger, so it is expected that TEM 1 and 11 yield the highest electricity conversion efficiency as they are exposed to the highest temperature, while TEMs 10 and 20 are exposed to the lowest temperatures in the heat exchanger and must yield the lowest electricity conversion efficiency.

2.4. Cooling system

A temperature gradient between the hot and cold surfaces of TEMs is required to generate electricity. While the hot surface is in contact with the external surface of the heat exchanger (i.e., upper

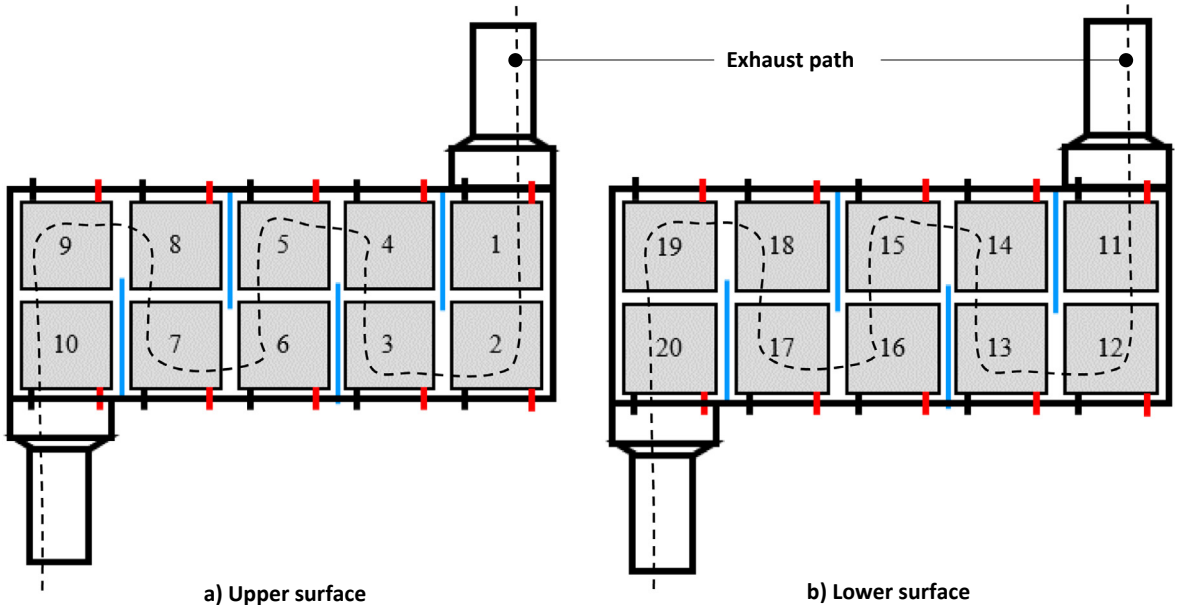

Fig. 5. Location of TEMs in the heat exchanger surfaces.

and lower surfaces, see Fig. 4), the cold surface is in contact with the cooling system. The cooling system is used to maintain a constant temperature on the cold surface during the experiments, in order to better control the experimental conditions. In practice, the cold surface is exposed, and it is cooled with the ambient air. The cooling system includes two rectangular coolers located on the cold surface of the TEMs (see Fig. 4). The coolant (i.e., water) was moved with a pump, while a chiller is used to remove the heat from the coolant.

2.5. Experimental facilities

A data acquisition system was used to measure and store the sensor data. The system includes a device to measure the temperature and a device to measure the currents and voltages in the TEMs. The input and output temperatures of the exhaust in the heat exchanger, and the water input and output temperatures in the cooling system are measured using K-type thermocouples and an analog to digital signal converter MAX6675 connected to an Arduino Mega 2560 microcontroller. Moreover, the currents and voltages of the 20 TEMs are measured using an electrical circuit connecting the TEMs with an Arduino Uno microcontroller and an Arduino Mega 2560.

The TEG is coupled to a stationary diesel engine in a test bench (see Fig. 6). The engine specifications are shown in Table 1.

The engine is coupled to an alternator controlled by a resistive test bench to control and measure the engine speed and torque.

The experimental facilities include two test benches coupled, namely: Diesel engine test bench, and the TEG test bench. The engine test bench includes a diesel engine, an alternator to control the engine's power output and the data acquisition system (DAQ) to control and measure the engine parameters. Moreover, the test bench of the TEG includes the heat exchanger, the TEM, the cooling system and a DAQ to control and measure the temperatures (inlet and outlet, of the exhaust gases and in the cooling system), the voltages and currents of each TEM. Between the test bench, there is a gas analyzer BrainBee AGS-688 (electromagnetic class E2) used to measure gaseous emissions, applying the international recommendation OIML R 99-1 & 2, which defines the instruments to measure exhaust emissions, the technical requirements, and the control of metrological and performance tests. In addition to this, the opacity of the exhaust gases is monitored with an opacimeter BrainBee OPA-100.

2.6. Experimental procedures

Nine different operational engine conditions were measured during the experiments. These conditions were selected to assess the impact of the TEG on energy efficiency and engine emissions. Each operational condition is guaranteed by controlling a dynamometric brake. The operational conditions were selected below the area of the engine characteristic curve to assess the most representative operating conditions of the engine. Fig. 7 shows the operating conditions selected.

Because fuel composition significantly affects the properties of the exhaust gases and emissions, the operation of the engine was measured using three different fuels: 1. Diesel, 2. Biodiesel blend (B5) and 3. Biodiesel blend (B10). Table 2 shows the physicochemical properties of the diesel and the biodiesel blends used.

An experimental design was conducted to determine two different effects of the engine parameters. The first effect is the

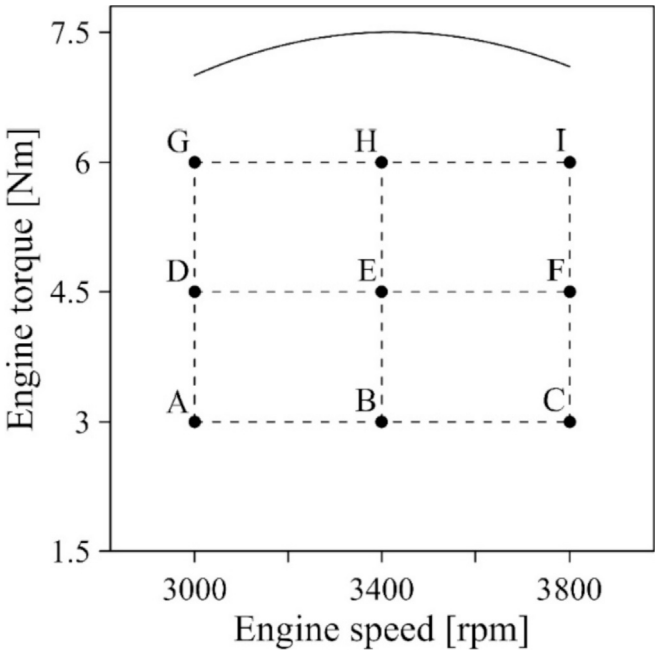

Fig. 7. Operational conditions of the engine selected for the experiments.

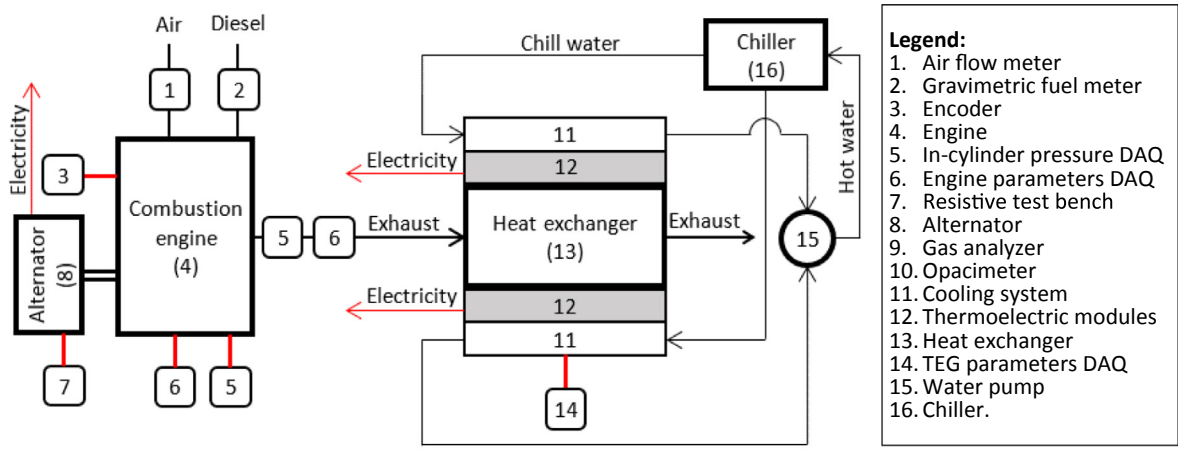

Fig. 6. Experimental facilities.

Table 2
Physicochemical properties of the fuels.

Property	Units	Standards	Diesel	B5	B10
Density	kg/m^3	ASTM D1298	821.5	823.1	827.5
Viscosity	cSt	ASTM D445	2.64	2.65	2.66
Flash point	°C	ASTM D93	76	85	96
Cloud point	°C	ASTM D2500	6.5	7.2	8.3
Pour point	°C	ASTM D97	3.1	3.5	3.8
NCP	MJ/kg	ASTM D240	44.05	43.89	43.25

Table 3
Response variables.

Response variables	Units	Symbol
TEG power	W	W
Carbon monoxide	ppm	CO
Carbon dioxide	%	CO_2
Nitrogen monoxide	ppm	NO
Nitrogen oxides	ppm	NO_X
Hydrocarbons	ppm	HC
Smoke opacity	HSU	S

engine parameters with type of fuel on the TEG performance and the second is the engine parameters on the ICE energy efficiency and emissions. The engine parameters considered are such as rotational speed and torque. The variables affecting the process performance were identified and classified into:

- Response variables: output variables to optimize
- Input variables: variables directly influencing the response variables
- Blocking variables: variables that are set in a fixed value. Its influence is out of the scope of the experiment.
- Noise variables: variables that are difficult to control and can modify the behavior of the response variables

The response variables identified are the TEG power and the gaseous emissions (see Table 3). The gaseous emissions of CO, CO_2, NO, NOx, HC, and smoke opacity were measured with a BrainBee AGS-688 and a BrainBee OPA-100 gas analyzer.

The input variables were the rotation speed, torque, and fuel blend (See Table 4). The minimum, middle, and maximum levels of these variables for each of the experimental design that was based on the operating conditions of the engine. Tables 4 and 5 show the variable levels and operating conditions used in the experiments.

The blocking variables are shown in Table 6.

The uncontrolled variables are shown in Table 7.

A multilevel factorial experimental design 3^3, including the three variable levels, was used. Thus, 27 experiments resulted in this case. Therefore, each measure is a unique combination of variables. In total, three repetitions were programmed for each condition, which resulted in 81 experiments. To ensure the randomness of the tests, and in order to eliminate the undesired effects introduced by environmental factors, the order of the experimental runs was defined using the STATGRAPHICS Centurion XVI.

The TEG operation was measured under steady-state conditions.

Table 5
Operational conditions.

Operational mode	Level	
	Torque	Rotational speed
B	B	M
C	B	A
D	M	B
E	M	M
F	M	A
G	A	B
H	A	M
I	A	A

Table 6
Blocking variables and noise variables.

Blocking variables	Unit	Symbol
Environmental temperature	°C	Te
Fuel temperature	°C	Tf
Air temperature dissipated	°C	Tad

Table 7
Uncontrolled variables.

Uncontrolled variables	Unit	Symbol
Cylinder head temperature	°C	Tc
Exhaust temperature	°C	Tex
Inlet pressure	kPa	Pa

Therefore, the data acquisition system started getting data once the exhaust temperatures at the inlet and outlet of the heat exchanger, and the cooling system temperatures varied within a range of ±0.2 °C during 5 min. After steady-state conditions were reached, the system measured the different variables for 3 min. The uncertainty in the temperature measurement with thermocouples type K is ±1.0 K and ±5% for the electrical resistances.

3. Results and discussion

There are different factors affecting the performance of TEGs. These factors are individually discussed in this section.

3.1. Engine load and temperature profile

Fig. 8 shows the temperature profile of the hot surface of the heat exchanger setting a cold surface temperature of 30 °C.

Results show that the temperature increases when the engine load increases for the three fuels. However, the increase of biodiesel in the fuel mixture increases the temperatures in the TEM. These results can be explained by the fact that higher engine loads lead to higher exhaust temperatures and higher flow rates. On the other hand, biodiesel has a higher oxygen availability for the air-fuel ratio, which causes high activation energy to complete the chemical reaction in the chamber. Also, biodiesel has a longer ignition that delays and slows the combustion rate. This can be attributed to its higher boiling point and viscosity than diesel, which causes

Table 4
Input variables.

Input variables	Units	Symbol	Minimum (B)	Middle (M)	Maximum (A)
Rotation speed	rpm	R	3000 rpm	3400 rpm	3800 rpm
Torque	Nm	T	3 Nm	4.5 Nm	6 Nm
Diesel-Biodiesel blends	%	B	0%	5%	10%

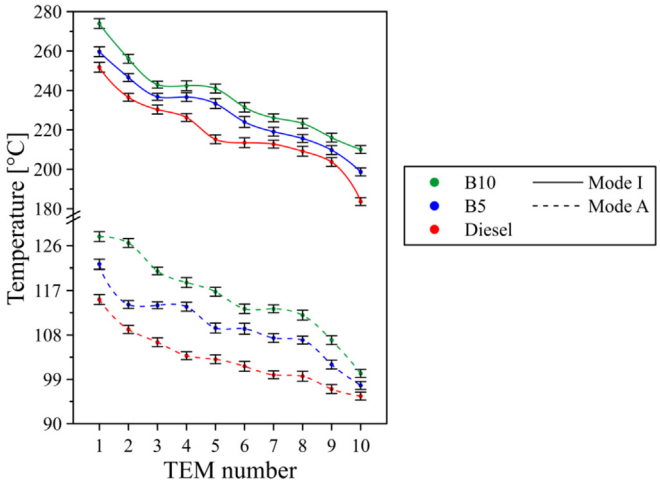

Fig. 8. Temperature profile in the heat exchanger.

incomplete evaporation in the main combustion phase while the fuel continues to burn in the late combustion phase. Diesel fuel has the lowest exhaust gas temperatures compared to biodiesel blends due to its higher calorific value and a shorter combustion phase. These results are aligned with the findings of (Raman et al., 2019) and (Ong et al., 2014).

The maximum exhaust gas temperature for diesel fuels, B5 and B10, was 252, 260 and 274 °C, respectively, under engine speed of 3800 rpm and torque of 6 Nm (mode I).

3.2. TEG power output

Fig. 9 shows the TEG power output for each operational condition considered, for the three fuels used.

The results show that the output power of the TEG increases with engine load and with the proportion of biodiesel in the fuel blends. This result is explained, on the one hand, by the higher exhaust temperature for higher engine loads, thus reducing the power input to the TEG. On the other hand, the lower NCP of biodiesel reduces the engine power output for higher biodiesel blends, also reducing the power input to the TEG. Since the cooling system is used for an experimental scenario (i. e. to keep constant the temperature of the cooling surface), the power used in this system is not considered in the energy balance of the TEG. Table 8 shows the net electrical power output of the TEG and the power loss due to the cooling system for the three fuel blends considered.

The highest power output was measured for operational mode I,

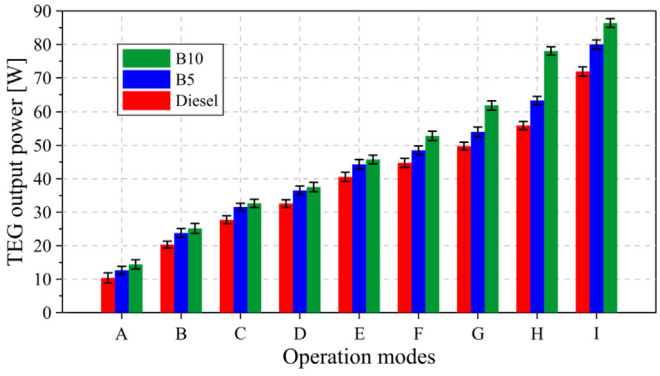

Fig. 9. TEG power output.

Table 8
Net electrical power and loss power.

Mode	Diesel		B5		B10	
	P_{net} (W)	P_{loss} (W)	P_{net} (W)	P_{loss} (W)	P_{net} (W)	P_{loss} (W)
A	5.52	4.86	7.42	5.24	8.80	5.61
B	13.23	7.09	16.26	7.53	17.15	7.97
C	19.31	8.40	22.72	8.82	23.40	9.24
D	23.39	9.18	26.96	9.56	27.61	9.95
E	30.23	10.33	33.67	10.64	34.83	10.94
F	33.85	10.89	37.35	11.18	41.35	11.47
G	38.23	11.53	42.17	11.86	49.61	12.18
H	43.62	12.27	50.32	12.90	64.51	13.53
I	57.87	14.01	65.37	14.64	71.13	15.27

accounting for 72 W for diesel, 80 W for B5, and 86 W for B10.

3.3. Pressure drop and conversion efficiency

Table 9 shows the pressure drop within the TEG for each operational mode of the engine, and for the three fuel blends considered. In addition, the energy conversion efficiency (i. e. the ratio between the power output and the heat absorbed in the TEG) used to evaluate the performance of the TEG is shown:

$$\eta = \frac{P_{out}}{\dot{m} \cdot c_p \cdot (T_{in} - T_{out})} \tag{9}$$

where η is the conversion efficiency, P_{output} is the TEG power output, $\dot{m}$ is the exhaust flow, c_p is the specific heat of the exhaust, T_{in} is the exhaust input temperature, and T_{out} is the exhaust output temperature.

Considering the temperature variation in the TEG, the variations of the exhaust specific heat can be neglected; thus, for simplicity, the specific heat of the exhaust is taken as:

- Diesel exhaust: $c_P = 1.017 \frac{J}{kg \cdot K}$
- B5 exhaust: $c_P = 1.015 \frac{J}{kg \cdot K}$
- B10 exhaust: $c_P = 1.014 \frac{J}{kg \cdot K}$

Results show that the pressure drop phenomenon increases with the engine load and speed, which is explained by the higher exhaust flow. Moreover, increasing the share of biodiesel in the fuel blend reduces the pressure drop, which might be explained by the higher flow of exhaust associated with diesel. The highest pressure drop registered in the experiments was of 1.2 kPa, which is a similar result of the simulation depicted in section 2.2. This backpressure is significantly lower than the maximum backpressure allowed by the engine (i.e., 2 kPa), so it is safe to install TEG in the engine exhaust system. In total, a pressure drop of 1 kPa causes a power loss of 15.27 W in the engine under 30% of the power recovered in

Table 9
Pressure drop and conversion efficiency.

Mode	Diesel		B5		B10	
	ΔP (kPa)	η (%)	ΔP (kPa)	η (%)	ΔP (kPa)	η (%)
A	0.54	2.28	0.45	2.36	0.41	2.46
B	0.80	2.31	0.66	2.42	0.58	2.60
C	0.86	2.33	0.74	2.47	0.67	2.69
D	0.89	2.35	0.81	2.50	0.73	2.77
E	0.98	2.36	0.86	2.53	0.81	2.83
F	1.00	2.37	0.90	2.55	0.85	2.88
G	1.05	2.39	0.96	2.58	0.90	2.93
H	1.07	2.39	1.00	2.59	0.93	2.97
I	1.20	2.40	1.08	2.61	1.00	3.00

Table 10
Effect of TEG implementation on emissions.

Fuel	Emission											
	CO (g/kWh)		CO_2 (g/kWh)		NO (g/kWh)		NOx (g/kWh)		HC (g/kWh)		Opacity (HSU)	
	T	WT	T	WT	T	WT	T	WT	T	WT	T	WT
Diesel	6.16	6.31	407.57	417.67	2.34	2.39	2.36	2.43	0.071	0.072	27.31	27.98
B5	5.24	5.39	370.73	380.82	2.11	2.16	2.62	2.70	0.063	0.065	24.34	25.00
B10	4.46	4.60	336.80	347.22	1.89	1.96	2.90	2.99	0.056	0.058	21.36	22.02

*T-with TEG; WT-without TEG.

operational mode I.

Overall, the conversion efficiency varies between 2.46 and 3% for B10, while for B5 varies between 2.36 and 2.61%, and for diesel between 2.28 and 2.4%. The highest efficiency was obtained for B10 in the operational model (i.e., 3800 rpm and 6 Nm of torque). As can be expected, the conversion efficiency of TEG increases with the engine load and speed.

3.4. Engine emissions

The implementation of the TEG resulted in lower fuel consumptions and it has the collateral benefit of reducing gaseous emissions. This section discusses the emission reduction of CO, CO_2, NO, NO_X, HC, and the opacity. Table 10 shows the results of emission measurements for the operation mode I.

It is shown that the average CO emissions of B5 and B10 were 15% and 27% lower than Diesel (see Table 10). This is due to the higher oxygen content of biodiesel results in more complete combustion, and thus in lower CO emissions. Similarly, the average CO_2 emissions of B5 and B10 were 9% and 16% lower than Diesel. This is attributed to the lower carbon percentage of biodiesel versus the diesel. Overall, reductions of 2.81% for CO and 2.76% for CO_2 emissions were obtained in the engine from the implementation of the TEG.

On average, it is observed 9% lower emissions of NO for B5 and 18% for B10 as compared to diesel emissions Moreover, the average NOx emissions of B5 is 11% higher than the emissions from diesel, while B10 is 23% higher. These results are in agreement with other studies that point to the higher oxygen content of biodiesel as the reason for an increase in emissions of NO_X (Palash et al., 2013). In general, higher oxygen contents result in higher combustion temperatures, leading to higher NO_X emissions (Kalam and Masjuki, 2002). The adiabatic flame temperature of pure biodiesel is 175 °C higher than the adiabatic flame temperature of diesel (Mao et al., 2011). Overall, the implementation of the TEG reduced in the emissions of NO and NOx in 2.42% for diesel, 2.66% for B5, and 3.26% for B10.

It is observed that HC emissions decrease with the increase of biodiesel in the blend. The higher oxygen content of biodiesel that promotes complete combustion reduces HC emissions. The average HC emissions were 10% lower for B5 and 19% lower for B10 as compared to Diesel.

The use of biodiesel blends resulted in lower smoke opacity when compared to Diesel, which is explained by the higher oxygen content in biodiesel, resulting in complete combustion, thus reducing the formation of smoke. On average, the combustion of B5 results in 11% less smoke than the combustion of diesel, while B10 resulted in 21% less smoke.

4. Conclusions

The internal geometry of the heat exchanger used in the thermoelectric generator is essential to guarantee its energy conversion efficiency. The offset strip fins heat exchanger has a higher heat transfer coefficient than the rectangular and waffle heat exchangers. However, it causes a pressure drop of over 2 kPa. The waffle heat exchanger introduces a maximum pressure drop of 1.2 kPa that causes a backpressure in the engine, inducing a power loss of 25%–30% of the power recovered in the TEG.

Increasing the biodiesel share in diesel blends reduces airborne emissions as compared to the use of diesel, although the emissions of NOX are increased. The use of B10 resulted in some 25% lower CO, CO_2, NO, HC, and smoke opacity emissions as compared to diesel, although increasing NOx emissions up to 23%. Moreover, biodiesel increases the temperature of the exhaust gases, which explains the fact using B5 and B10 results in 12 and 23% higher values of power output in the TEG, than using diesel. Overall, when using diesel, the TEG had up to 2.42% of recovery efficiency, while using B5 was 2.65%, and using B10 was 3%.

Declarations of interest

None.

Acknowledgments

The authors want to acknowledge the support of the Universidad del Atlántico and Sphere Energy company on the development of this research by providing access to their facility.

References

Alagumalai, A., 2014. Internal combustion engines: Progress and prospects. Renew. Sustain. Energy Rev. 38, 561–571.
Aranguren, P., Araiz, M., Astrain, D., Martínez, A., 2017. Thermoelectric generators for waste heat harvesting: a computational and experimental approach. Energy Convers. Manag. 148, 680–691.
Darda, S., Papalas, T., Zabaniotou, A., 2019. Biofuels journey in Europe: currently the way to low carbon economy sustainability is still a challenge. J. Clean. Prod. 208, 575–588.
He, W., Wang, S., 2017. Thermoelectric performance optimization when considering engine power loss caused by back pressure applied to engine exhaust waste heat recovery. Energy 133, 584–592.
He, W., Wang, S., Zhang, X., Li, Y., Lu, C., 2015. Optimization design method of thermoelectric generator based on exhaust gas parameters for recovery of engine waste heat. Energy 91, 1–9.
In, B.D., Kim, H.I., Son, J.W., Lee, K.H., 2015. The study of a thermoelectric generator with various thermal conditions of exhaust gas from a diesel engine. Int. J. Heat Mass Transf. 86, 667–680.
Kalam, M.A., Masjuki, H.H., 2002. Biodiesel from palmoil - an analysis of its properties and potential. Biomass Bioenergy 23, 471–479.
Kim, T.Y., Negash, A., Cho, G., 2017. Direct contact thermoelectric generator (DCTEG): a concept for removing the contact resistance between thermoelectric modules and heat source. Energy Convers. Manag. 142, 20–27.
Kim, T.Y., Negash, A.A., Cho, G., 2016. Waste heat recovery of a diesel engine using a thermoelectric generator equipped with customized thermoelectric modules. Energy Convers. Manag. 124, 280–286.
Kiziroglou, M.E., Wright, S.W., Toh, T.T., Mitcheson, P.D., Becker, T., Yeatman, E.M., 2014. Design and fabrication of heat storage thermoelectric harvesting devices. IEEE Trans. Ind. Electron. 61, 302–309.
Lan, S., Yang, Z., Chen, R., Stobart, R., 2018. A dynamic model for thermoelectric generator applied to vehicle waste heat recovery. Appl. Energy 210, 327–338.
Lee, H., 2010. Thermal Design: Heat Sinks, Thermoelectrics, Heat Pipes, Compact Heat Exchangers, and Solar Cells. John Wiley & Sons, Hoboken, New Jersey.

Li, W., Paul, M.C., Siviter, J., Montecucco, A., Knox, A.R., Sweet, T., Min, G., Baig, H., Mallick, T.K., Han, G., Gregory, D.H., Azough, F., Freer, R., 2016. Thermal performance of two heat exchangers for thermoelectric generators. Case Stud. Therm. Eng. 8, 164–175.

Lion, S., Michos, C.N., Vlaskos, I., Rouaud, C., Taccani, R., 2017. A review of waste heat recovery and Organic Rankine Cycles (ORC) in on-off highway vehicle Heavy Duty Diesel Engine applications. Renew. Sustain. Energy Rev. 79, 691–708.

Love, N.D., Szybist, J.P., Sluder, C.S., 2012. Effect of heat exchanger material and fouling on thermoelectric exhaust heat recovery. Appl. Energy 89, 322–328.

Mao, G., Wang, Z., Hu, P., Ni, P., Wang, X., Gu, S.Q., 2011. Experimental research on the flame temperature of biodiesel fuel combustion in open-air conditions. In: 2011 International Conference on Electric Information and Control Engineering, ICEICE 2011 - Proceedings, pp. 2171–2174.

Niu, Z., Diao, H., Yu, S., Jiao, K., Du, Q., Shu, G., 2014. Investigation and design optimization of exhaust-based thermoelectric generator system for internal combustion engine. Energy Convers. Manag. 85, 85–101.

Ong, H.C., Masjuki, H.H., Mahlia, T.M.I., Silitonga, A.S., Chong, W.T., Yusaf, T., 2014. Engine performance and emissions using Jatropha curcas, Ceiba pentandra and Calophyllum inophyllum biodiesel in a CI diesel engine. Energy 69, 427–445.

Osorio, J.D., Rivera-Alvarez, A., 2018. Efficiency enhancement of spark-ignition engines using a Continuous Variable Valve Timing system for load control. Energy 161, 649–662.

Palash, S.M., Kalam, M.A., Masjuki, H.H., Masum, B.M., Rizwanul Fattah, I.M., Mofijur, M., 2013. Impacts of biodiesel combustion on NOx emissions and their reduction approaches. Renew. Sustain. Energy Rev. 23, 473–490.

Patil, D.S., Arakerimath, R.R., Walke, P.V., 2018. Thermoelectric materials and heat exchangers for power generation – a review. Renew. Sustain. Energy Rev. 95, 1–22.

Raman, L.A., Deepanraj, B., Rajakumar, S., Sivasubramanian, V., 2019. Experimental investigation on performance, combustion and emission analysis of a direct injection diesel engine fuelled with rapeseed oil biodiesel. Fuel 69–74.

Rimkus, A., Melaika, M., Matijošius, J., 2017. Efficient and ecological indicators of CI engine fuelled with different diesel and LPG mixtures. In: Procedia Engineering. Elsevier Ltd, pp. 504–512.

Su, C.Q., Wang, W.S., Liu, X., Deng, Y.D., 2014. Simulation and experimental study on thermal optimization of the heat exchanger for automotive exhaust-based thermoelectric generators. Case Stud. Therm. Eng. 4, 85–91.

Temizer, I., Ilkiliç, C., 2016. The performance and analysis of the thermoelectric generator system used in diesel engines. Renew. Sustain. Energy Rev. 63, 141–151.

Vale, S., Heber, L., Coelho, P.J., Silva, C.M., 2017. Parametric study of a thermoelectric generator system for exhaust gas energy recovery in diesel road freight transportation. Energy Convers. Manag. 133, 167–177.

Verma, S., Das, L.M., Bhatti, S.S., Kaushik, S.C., 2017. A comparative exergetic performance and emission analysis of pilot diesel dual-fuel engine with biogas, CNG and hydrogen as main fuels. Energy Convers. Manag. 151, 764–777.

Zavaragh, H.G., Kaleli, A., Afshari, F., Amini, A., 2017. Optimization of heat transfer and efficiency of engine via air bubble injection inside engine cooling system. Appl. Therm. Eng. 123, 390–402.